DALTON

Dinuclear iron(III)–metal(II) complexes as structural core models for purple acid phosphatases †

Morten Ghiladi,[a,c] Christine J. McKenzie,*[,a] Anke Meier,[a] Annie K. Powell,[b] Jens Ulstrup[c] and Sigrid Wocadlo[b]

[a] *Department of Chemistry, Odense University, DK-5230 Odense M, Denmark*
[b] *Department of Chemistry, University of East Anglia, Norwich, UK NR4 7TJ*
[c] *Department of Chemistry, The Technical University of Denmark, DK-2800 Lyngby, Denmark*

A series of mixed-valent iron and mixed-metal Fe^{III}–M^{II} (M = Zn, Cu, Ni or Co) complexes of the phenolate-hinged dinucleating ligand 2,6-bis{[bis(2-pyridylmethyl)amino]methyl}-4-*tert*-butylphenolato(1−), $bpbp^-$ have been prepared and characterized. Both exogenous bidentate bridging groups and different terminal ligands bound to each different metal ion at the exogenous site were identified. The structure of the mixed-valence complex $[(bpbp)Fe_2(F)_2(H_2O)_2][BF_4]_2$ confirms that it is a rare example of a dimetallic complex of a single-atom hinged acyclic dinucleating ligand with a 'non-bridged' arrangement at the exogenous bridging site. Mössbauer spectroscopy indicates valence trapping in this complex with the parameters, ΔE_Q 3.242 mm s^{-1}, δ 1.169 mm s^{-1} and ΔE_Q 0.221 mm s^{-1}, δ 0.460 mm s^{-1}, respectively for the high spin Fe^{2+} and high spin Fe^{3+} ions. Crystals of $[(bpbp)Fe_2(F)_2(H_2O)_2][BF_4]_2\cdot 4H_2O$ are triclinic, space group $P\bar{1}$ (no. 2), with a = 12.695(1), b = 19.197(2), c = 10.202(1) Å, α = 102.95(1), β = 97.61(1), γ = 93.76(1)°, Z = 2. The structure was refined to R = 0.1009 on F using 4338 reflections with $I > 2\sigma(I)$ (*wR*2 on all data and F^2 = 0.3522). The Fe^{II} and Fe^{III} atoms are bridged asymmetrically by the phenolic oxygen atom of $bpbp^-$ with Fe^{II}–O 2.175(6) Å and Fe^{III}–O 2.033(6) Å with a $Fe^{III}\cdots Fe^{II}$ distance of 3.726(2) Å. The two terminal fluoride ions are bound to the Fe^{III} atom and strongly hydrogen bonded to two water molecules bound to the adjacent Fe^{II} atom. This complex may model the mode in which fluoride ions bind to the active site of the purple acid phosphatases (PAPs) thereby inhibiting the activity of these enzymes. Tetrahedral oxo anions are known also to inhibit PAPs and to mimic this inhibition a Fe^{III}–Zn^{II} complex incorporating molybdate bridging groups was prepared. Crystals of $[(bpbp)FeZn(MoO_4)_2]\cdot C_3H_7OH\cdot 2H_2O$ are monoclinic, space group $P2_1/n$ with a = 11.773(13), b = 21.394(7), c = 17.001(11) Å and β = 90.98(7)°, Z = 4. The structure was refined to R = 0.0434 on F using 3758 reflections with $I > 2\sigma(I)$ (*wR*2 on all data and F^2 = 0.1339). The $Fe^{III}\cdots Zn^{II}$ distance is 3.819(4) Å. A series of acetate-bridged complexes were prepared by the novel method of diffusing ethyl acetate or isopropyl acetate into mixtures of Hbpbp and iron perchlorate in the presence and absence of a second type of metal ion. The acetate bridging groups are the result of the hydrolysis of the alkyl acetate. These complexes have the general formulation $[(bpbp)FeM(CH_3CO_2)_2][ClO_4]_2$. Crystals of $[(bpbp)FeCu(CH_3CO_2)_2][ClO_4]_2\cdot 0.5CH_3OH$ are monoclinic, space group $P2_1/n$ with a = 12.677(2), b = 22.059(2), c = 16.269(2) Å and β = 94.184(1)°, Z = 4. The structure was refined to R = 0.0538 on F using 5097 reflections with $I > 2\sigma(I)$ (*wR*2 on all data and F^2 = 0.2684). The $Fe^{III}\cdots Cu^{II}$ distance is 3.419(2) Å. Asymmetrical bridging by the hinging phenolate group is evident in the bis(molybdate)-bridged Fe–Zn complex and the bis(acetate)-bridged Fe–Cu complex, however it is significantly less pronounced compared with the 'non-bridged' fluoride containing Fe^{III}–Fe^{II} complex. While the fluoride and molybdate complexes may model aspects of the binding of these ions in inhibited PAPs, the generation of acetate complexes from the hydrolysis of alkyl esters may indeed model part of the reactivity of PAPs. However, we have unfortunately not been able to ascertain that this reaction is promoted by the metal complexes.

The study of heterodimetallic complexes is interesting in regard to their potential in modelling the structures and reactivities of metalloenzymes containing two different metal ions at their active sites, as well as the possible discovery of new types of co-operative heterodimetallic activation chemistry and the implications this has in the study of the magnetic and electronic interactions in such systems. However the preparation of mixed-metal complexes is often a considerable challenge. In one approach several groups have utilized the ability of macrocyclic[1] and acyclic[2] phenolate-hinged ligands to stabilize both mixed-metal and mixed-valent complexes. In an extension of this work we now describe diiron(II/III) and heterodimetallic complexes of the acyclic phenolate-hinged dinucleating ligand, 2,6-bis{[bis(2-pyridylmethyl)amino]methyl}-4-*tert*-butylphenolato(1−), $bpbp^-$. The $bpbp^-$ ligand stabilizes complexes containing one trivalent and one divalent metal ion thus both mixed-metal and mixed-valent systems are accessible.

The active site of red kidney bean purple acid phosphatase (RKBPAP) contains a Zn^{2+} and an Fe^{3+} ion, while those of the mammalian purple acid phosphatases isolated from beef spleen (BSPAP) and porcine uterus (also called uteroferrin, Uf) contain an Fe^{3+} and an Fe^{2+} ion in their functional forms. A single oxygen atom from the carboxylate group of Asp-164 (Asp = aspartic acid) was found to be the endogenous bridging atom between the Fe^{III} and the Zn^{II} atoms in the recent crystal structure of RKPAP.[3] Beef spleen purple acid phosphatase and Uf probably have related structures. The dinucleating ligand $bpbp^-$ used for the complexes described here thus holds important physical features in common with the PAP enzymes since dimetallic complexes with a single-atom negatively-charged endogenous hinge as well as M^{III}–M^{II} systems can be prepared.

Que and co-workers[2b,f,g] have reported a series of complexes in which oxo acids such as carboxylates bridge the two metal

† Based on the presentation given at Dalton Discussion No. 2, 2nd–5th September 1997, University of East Anglia, UK.

ions in the dimetallic complexes of the closely related ligand, 2,6-bis{[*N*,*N*-bis(2-methylpyridine)amino]methyl}-4-methylphenolato(1−), bpmp$^-$. We have concentrated on the preparation of corresponding 'non-bridged' systems in which the co-ordination spheres of the metal atoms are completed, either exclusively or predominantly, by water and water-derived ligands. Such systems are potentially interesting for the study of biologically relevant substitution and hydrolysis reactions. Specifically, complexes containing cations of formulation $[(bpbp)Fe_2(OH)_n(H_2O)_{4-n}]^{(4-n)+}$ were desirable. Precedence for such iron complexes with terminal hydroxide ligands, *e.g.* $[(bpbp)Fe_2(OH)_n(H_2O)_{4-n}]^{(4-n)+}$ ($n = 2$) comes from some of our earlier work in which we reported the μ-oxide complex [(tpa)(OH)Fe(μ-O)Fe(H_2O)(tpa)][ClO_4]$_3$ [tpa = tris(2-methylpyridyl)amine] which is the first example of a non-porphyrin iron(III) complex with a terminal hydroxide ligand.[4] Interestingly, this particular complex shows biologically relevant reactivity; it promotes the hydrolyses of triphenyl phosphate and acetonitrile. The diphenyl phosphate- and acetamide-bridged complexes [(tpa)Fe(μ-O){μ-$O_2P(OPh)_2$}Fe(tpa)][ClO_4]$_3$ and [(tpa)Fe(μ-O)(μ-CH_3CONH)Fe(tpa)][ClO_4] respectively are isolated from these reactions. In further studies of this type of reactivity, related systems based on a single endogenous ligand are appropriate, hence the choice of bpbp$^-$. Of course there are electronic differences between oxide (charge, 2−)-bridged and phenolate (charge, 1−)-hinged complexes. The difference in the charge of the linking oxygen atoms is apparently compensated for by the fact that Fe^{III}–Fe^{II} is the favored oxidation state for the phenolate-hinged systems while the Fe^{III}–Fe^{III} oxidation state is favored in oxide-bridged complexes. Thus the overall Lewis acidity of the $[(bpbp)Fe^{III}Fe^{II}]^{4+}$ unit may, in fact, be rather similar to the $[(tpa)Fe^{III}OFe^{III}(tpa)]^{4+}$ unit. As noted, the Fe^{III}–Fe^{II} systems are more relevant than the Fe^{III}–Fe^{III} systems for modelling PAPs.

A conceivable scenario for the reactivity of complexes such as $[(bpbp)Fe_2(OH)_n(H_2O)_{4-n}]^{(4-n)+}$ is the substitution of the water ligands by a substrate and its subsequent hydrolysis due to intramolecular attack by hydroxide co-ordinated to the adjacent metal atom. Similar reactivity has been reported earlier. A co-ordinated hydroxide ion was proposed as the nucleophile important in hydrolysis mechanisms for several dinuclear metal complexes (Co–Co,[5] Fe–Fe,[4,6] Cu–Cu,[7] Zn–Zn,[8] Pd–Pd[9] and La–La[10]) which catalyse the hydrolysis of several substrates, for example, phosphate esters,[4,5,8,10] amides[7] and nitriles.[4,5,6,9] This hydroxide ion is bound to one of the metal ions while the second metal ion is crucial for monodentate co-ordination and Lewis-acid activation of the substrate. These mechanisms are analogous to those postulated for hydrolysis catalysis by the dinuclear metalloenzymes, purple acid phosphatases, PAPs (Fe^{III}–Fe^{II}, Fe^{III}–Zn^{II}),[11] alkaline phosphatases (Zn^{II}–Zn^{II}–Mg^{II})[12] and urease (Ni^{III}–Ni^{II}).[13] A mechanism involving the double Lewis-acid activation of a bridging monophenylphosphate towards hydrolysis in the dicobalt(III) complex, [Co_2(bpmp){$O_3P(Ph)$}(H_2O)(OH)][ClO_4]$_2$, was also reported recently.[14] Analogous two-metal activation of the substrate may also be relevant to the function of the two metal ions in PAPs.

Purple acid phosphatases are known to be inhibited by fluoride and molybdate ions.[15] Presented here are fluoride and molybdate complexes based on the $[(bpbp)Fe^{III}M^{II}]^{4+}$ core which have been characterized crystallographically. These complexes may model aspects of the inhibition. The fluoride complex [(bpbp)$Fe_2(F)_2(H_2O)_2$][BF_4]$_2$ is a rare example of a complex in which the ligand occupying the exogenous bridging site of a dimetallic complex of an acyclic ligand is not a bidentate bridging ligand. The ligands bound to each metal ion are also different. The structure of [(bpbp)$Fe_2(F)_2(H_2O)_2$][BF_4]$_2$ is relevant not only as a model complex for fluoride inhibited PAP but also as a non-bridging system in which the ligand(s) on each metal ion are poised to react. This particular complex therefore illuminates the crucial initial step in dimetal catalysed processes; specific substrate co-ordination at a particular metal ion. For the dinuclear hydrolytic enzymes, the substrate is bound to one metal ion (after replacing a water ligand), and the hydroxide ion, to the other metal ion, in a non-bridged configuration. After reaction of substrate and hydroxide ion the resultant product may bridge the metal centers. Many model complexes for such a bidentate bridging arrangement have been reported, but complexes of dinucleating ligands in which the exogenous bridging site is 'non-bridged' are rare.[2k,16] The structural characterization of such species lends credence to catalytic mechanisms involving the condensation of different species bound to adjacent metals.

Experimental

Proton and ^{13}C NMR spectra were recorded on a Bruker AC 250, using $SiMe_4$ as an internal reference. Fluorine-19 NMR spectra were recorded on a Varian Gemini 2000 using α,α,α-trifluorotoluene as an internal reference. Elemental analyses were performed at the Chemistry Department II at Copenhagen University, Denmark and Atlantic Microlab, Inc., Norcross, GA, USA. Cyclic voltammograms were obtained using an Eco Chemie Autolab potentiostat equipped with an electron-capture detector low current auxiliary module. The data were acquired with a computer using the General Purpose Electrochemical Systems version 3.2 software (Eco Chemie software). The all-glass cell consisted of a working and a reference compartment connected *via* a Luggin capillary. The working compartment contained a platinum disc (5 mm in diameter) working electrode and a semi-cylindrical platinum gauze auxiliary electrode. The reference electrode consisted of a silver wire immersed in a 0.10 M solution of NBu_4PF_6 in dry acetonitrile which was 0.01 M in $AgNO_3$. The reference compartment was separated from the working solution by a Vycor plug. Dry acetonitrile was obtained from Aldrich Chemical Company, Inc. (>99.8%) and was used as received. All experiments were performed at ambient temperature in solutions of dry acetonitrile with 0.1 M tetrabutylammonium hexafluorophosphate as the supporting electrolyte. The ferrocenium–ferrocene couple was used to monitor the reference electrode potential which was found to be 89 mV. Spectroelectrochemical characterization of the preparations was undertaken using a locally constructed optically transparent thin-layer electrolysis (OTTLE) cell. The functional principles follow that of ref. 17. The design is based on a construction provided by Gray[18] but material and design are modified to cope with the organic solvents used. The cell was made of Teflon, with quartz windows. A set of thin glass tubes ensured facile inlet of solution and rinsing of the cell. The working electrode was an optically transparent thin gold film. The reference electrode was the same as that used for the cyclic voltammetry experiments. The counter electrode was a platinum wire. The cell was mounted in a Hewlett-Packard 8453 diode array spectrophotometer and absorption spectra recorded in parallel with the electrochemical control.

The UV/VIS spectra were recorded on a Shimadzu UV-3100 spectrophotometer using 1.0 cm quartz cuvettes. Infrared spectra of the complexes in KBr discs were measured using a Hitachi 270-30 IR spectrometer. The pH was measured with a Radiometer pHC2201 combined pH electrode with a double liquid junction (inner liquid junction: saturated aqueous KCl, outer liquid junction: saturated aqueous $NaClO_4$). Fast atom bombardment mass spectra (FAB mass spectra) were recorded on a Kratos MS50TC spectrometer and electrospray ionization mass spectra (ES mass spectra) were obtained using a Finnigan TSQ 700 triple quadrupole instrument equipped with a Finnigan API source in the electrospray mode using acetonitrile solutions. **CAUTION!** Although no problems were encountered in the preparation of the perchlorate salts care

should be taken when handling such potentially hazardous compounds.

2,6-Bis{[bis(2-pyridylmethyl)amino]methyl}-4-*tert*-butylphenol, Hbpbp

4-*tert*-Butylphenol (1.994 g, 0.0133 mol) and *p*-formaldehyde (1.55 g, 0.0517 mol) were suspended in ethanol (25 cm^3). A solution of *N*,*N*-bis(2-pyridylmethyl)amine (10.0 g, 0.0503 mol) in H_2O (50 cm^3) was added and the slightly yellow suspension was stirred at reflux temperature for 3 d. The two-phase reaction mixture was allowed to cool to room temperature and was then partitioned between CH_2Cl_2 (200 cm^3) and H_2O (100 cm^3). The aqueous phase was extracted with CH_2Cl_2 (3 × 50 cm^3) and the combined organic phase dried over anhydrous Na_2SO_4. After removal of the solvent, the resulting brown oil was chromatographed on a silica gel column using acetone as eluent affording the crude product (5.86 g, 77% yield) as a slightly yellow solid (m.p. = 122–126 °C). Recrystallization from diethyl ether–light petroleum resulted in the pure product as white crystals (60% relative to the crude product, m.p. = 123 °C). ^{1}H NMR (250 MHz): δ 1.27 (s, 9 H), 3.82 (s, 4 H), 3.90 (s, 8 H), 7.08 (m, 4 H), 7.19 (s, 2 H), 7.48–7.61 (m, 8 H), 8.52 (m, 4 H), 10.80 (s, 1 H). ^{13}C-{^{1}H} NMR (62 MHz): δ 31.57 (s), 33.85 (s), 55.12 (s), 59.88 (s), 121.81 (s), 122.84 (s), 123.16 (s), 125.85 (s), 136.33 (s), 140.79 (s), 148.83 (s), 153.43 (s), 159.39 (s) (Found: C, 75.49; H, 7.04; N, 14.67. Calc. for $C_{36}H_{40}N_6O$: C, 75.23; H, 6.96; N, 14.48%). FAB mass spectrum: *m*/*z* 572 (0.5, M^+), 93 (100%, $C_5H_4NCH_2^+$).

$[(bpbp)Fe_2(F)_2(H_2O)_2][BF_4]_2$

A solution of Hbpbp (0.1348 g, 0.23 mmol) in acetone (2 cm^3) was mixed with $Fe(BF_4)_2{\cdot}6H_2O$ (0.1985 g, 0.59 mmol) dissolved in water (8 cm^3). The color of the reaction mixture changed from deep brown to purple red within 1 h on standing. Dark blue crystals of $[(bpbp)Fe_2(F)_2(H_2O)_2][BF_4]_2$ in 95% yield were deposited after standing overnight in an open vessel. These were collected and dried in vacuum at room temperature for 12 h (Found: C, 46.69; H, 4.76; N, 9.04. Calc. for $C_{36}H_{43}B_2F_{10}Fe_2N_6O_3$: C, 46.44; H, 4.66; N, 9.03%). FAB mass spectrum: *m*/*z* 721 {100, $[(bpbp)Fe_2(F)_2]^+$}, 740 {90%, $[(bpbp)Fe_2(F)_2(H_2O)]^+$}. ^{19}F NMR (300 MHz): δ 3.2 (s), 75.8 (s). UV/VIS (CH_3CN) λ_{max}/nm (ε/dm^3 mol^{-1} cm^{-1}): 254 (1714) 301 (806), 356 (403).

$[(bpbp)FeZn(MoO_4)_2]$

A solution of Hbpbp (0.0518 g, 0.09 mmol) in methanol (5 cm^3) was added to a solution of $Fe(ClO_4)_3{\cdot}6H_2O$ (0.032 g, 0.09 mmol) in H_2O (5 cm^3) and $Zn(ClO_4)_2{\cdot}6H_2O$ (0.0337 g, 0.09 mmol) was subsequently added. The resulting purple mixture was stirred vigorously at reflux temperature and a solution of $Na_2[MoO_4]$ (0.044 g, 0.18 mmol) in H_2O (2 cm^3) was added dropwise. The color of the mixture changed to a more intense purple and the product was isolated as a blue microcrystalline solid in quantitative yield (Found: C, 42.51; H, 3.92; N, 8.32. Calc. for $C_{36}H_{39}FeMo_2N_6O_9Zn$: C, 42.69; H, 3.88; N, 8.30%). UV/VIS (1:1 ethanol–CH_2Cl_2) λ_{max}/nm (ε/dm^3 mol^{-1} cm^{-1}): 256 (1.87 × 10^4), 302 (sh, 7060), 334 (sh, 5855), 520 (518). Recrystallization from a 3:1 mixture of propan-2-ol and H_2O afforded crystals suitable for X-ray crystallography.

$[(bpbp)FeM(CH_3CO_2)_2][ClO_4]_2$ (M = Co, Ni, Cu, Zn or Fe)

In a typical experiment a solution of Hbpbp (0.3000 g, 0.52 mmol) in methanol (2 cm^3) was added to a solution of $Fe(ClO_4)_3{\cdot}6H_2O$ (0.1854 g, 0.52 mmol) in H_2O (10 cm^3). One equivalent of the appropriate $M(ClO_4)_2{\cdot}nH_2O$ was then added. Slow diffusion of either ethyl acetate or isopropyl acetate into the reaction mixture afforded the product in a quantitative yield within 2 d (Found: C, 46.97; H, 4.54; Cl, 7.15; N, 8.22. Calc. for $C_{40}H_{45}Cl_2CoFeN_6O_{13}$: C, 47.88; H, 4.52; Cl, 7.07; N, 8.37%). ES mass spectrum: *m*/*z* 402.3 {100%, $[(bpbp)FeCo(CH_3CO_2)_2]^{2+}$}. UV/VIS ($CH_3CN$) λ_{max}/nm (ε/dm^3 mol^{-1} cm^{-1}): 253 (1.93 × 10^4), 368 (sh, 1784), 442 (sh, 1113), 588 (sh, 885) (Found: C, 46.74; H, 4.53; Cl, 7.08; N, 8.25. Calc. for $C_{40}H_{45}Cl_2FeN_6NiO_{13}$: C, 47.89; H, 4.52; Cl, 7.07; N, 8.38%). ES mass spectrum: *m*/*z* 401.8 {100%, $[(bpbp)FeNi(CH_3CO_2)_2]^{2+}$}. UV/VIS ($CH_3CN$) λ_{max}/nm (ε/dm^3 mol^{-1} cm^{-1}): 253 (1.66 × 10^4), 290 (sh, 6470), 378 (sh, 1344), 560 (806) (Found: C, 47.15; H, 4.51; Cl, 7.00; N, 8.35. Calc. for $C_{40}H_{45}Cl_2CuFeN_6O_{13}$: C, 47.66; H, 4.50; Cl, 7.03; N, 8.34%). ES mass spectrum: *m*/*z* 404.3 {100%, $[(bpbp)FeCu(CH_3CO_2)_2]^{2+}$}. UV/VIS ($CH_3CN$) λ_{max}/nm (ε/dm^3 mol^{-1} cm^{-1}): 255 (2.07 × 10^4), 289 (sh, 9218), 326 (sh, 4483), 551 (776) (Found: C, 45.84; H, 4.43; Cl, 7.48; N, 8.15. Calc. for $C_{40}H_{45}Cl_2FeN_6O_{13}$: C, 47.57; H, 4.49; Cl, 7.02; N, 8.32%). ES mass spectrum: *m*/*z* 404.8 {100%, $[(bpbp)FeZn(CH_3CO_2)_2]^{2+}$}. UV/VIS ($CH_3CN$) λ_{max}/nm (ε/dm^3 mol^{-1} cm^{-1}): 258 (1.74 × 10^4), 295 (sh, 6313), 366 (sh, 2003), 558 (793) (Found: C, 45.32; H, 4.52; Cl, 7.31; N, 7.94. Calc. for $C_{40}H_{45}Cl_2Fe_2N_6O_{13}$: C, 48.02; H, 4.53; Cl, 7.09; N, 8.40%). FAB mass spectrum: *m*/*z* 801 {100, $[(bpbp)Fe_2(CH_3CO_2)_2]^+$}, 900 (45%, $\{[(bpbp)Fe_2(CH_3CO_2)_2][ClO_4]\}^+$). UV/VIS ($CH_3CN$) λ_{max}/nm (ε/dm^3 mol^{-1} cm^{-1}): 256 (2.19 × 10^4), 296 (sh, 8438), 329 (sh, 5141), 381 (sh, 3000), 555 (1036).

X-Ray crystallography

The structures of $[(bpbp)Fe_2(F)_2(H_2O)_2][BF_4]_2{\cdot}4H_2O$ **1**, $[(bpbp)FeZn(MoO_4)_2]{\cdot}C_3H_7OH{\cdot}2H_2O$ **2** and $[(bpbp)FeCu(CH_3CO_2)_2][ClO_4]_2{\cdot}0.5CH_3OH$ **3** were determined by single-crystal X-ray diffraction on a Rigaku AFC7R diffractometer. Data were collected at low temperature with mounted crystals cooled directly in the nitrogen stream of an Oxford Instruments Cryostream cooling device. Structures were solved and refined using the SHELXTL PLUS[19] and SHELXL 93[20] programs. In all cases the refinements proceeded smoothly. Table 1 contains the crystal data and further details of the X-ray structural determinations. Selected bond distances and angles are listed in Table 2.

CCDC reference number 186/669.

Results and Discussion

Attempts to prepare complexes containing the cations $[(bpbp)Fe_2(OH)_n(H_2O)_{4-n}]^{(4-n)+}$

The reaction of Hbpbp with iron salts in various solvent–water mixtures in the absence of potential bridging ligands was attempted with the hope of isolating complexes containing cations of formulation $[(bpbp)Fe_2(OH)_n(H_2O)_{4-n}]^{(4-n)+}$ (n = 1–4). We were unfortunately unable to characterize any such complex from the reactions of Hbpbp with iron tetrafluoroborate or iron perchlorate, however the cation in the fluoride complex, $[(bpbp)Fe_2(F)_2(H_2O)_2][BF_4]_2$, described below is isoelectronic with $[(bpbp)Fe_2(OH)_n(H_2O)_{4-n}]^{(4-n)+}$ (n = 2).

The reaction of Hbpbp with 2 equivalents of either iron(II)- or iron(III)-perchlorate generates deep blue solutions from which a brown-red crystalline product can be isolated. The formulation of the brown-red crystals is not satisfactorily assigned at this stage although we believe this to be a tetranuclear iron complex containing two $bpbp^-$ ligands and four (hydr)oxo bridging groups. A base peak at *m*/*z* 477 (triply-charged ion) in the ES mass spectrum of this material can be assigned to $[(bpbp)_2Fe^{III}{}_4O_4H]^{3+}$. This ion or a close relative may be the cation in the isolated complex. Complete structural elucidation awaits the growth of crystals suitable for X-ray analysis. Since the formulation of this complex is ambiguous at the present time it has not been included in the Experimental section.

The formation of the above mentioned red solid product from the mixtures of iron perchlorate and Hbpbp is pH dependent and below approximately pH 5 this material could

Table 1 Crystal data and details of structural determinations

Compound	[(bpbp)$Fe_2(F)_2(H_2O)_2$][BF_4]$_2$·$4H_2O$ **1**	[(bpbp)$FeZn(MoO_4)_2$]·C_3H_7OH·$2H_2O$ **2**	[(bpbp)$FeCu(CH_3CO_2)_2$][ClO_4]$_2$·$0.5CH_3OH$ **3**
Empirical formula	$C_{36}H_{51}B_2F_{10}Fe_2N_6O_7$	$C_{39}H_{51}FeMo_2N_6O_{12}Zn$	$C_{40.5}H_{47}Cl_2CuFeN_6O_{13.5}$
M	1003.15	1108.96	1023.63
T/K	223(2)	233(2)	233(2)
λ/Å	0.710 69	0.710 69	0.710 69
Crystal system	Triclinic	Monoclinic	Monoclinic
Space group	$P\bar{1}$ (no. 2)	$P2_1n$	$P2_1/n$
a/Å	12.6950(10)	11.773(13)	12.677(2)
b/Å	19.197(2)	21.394(7)	22.059(2)
c/Å	10.2020(10)	17.001(11)	16.269(2)
α/°	102.955(10)		
β/°	97.609(10)	90.98(7)	94.184(1)
γ/°	93.766(10)		
U/Å^3, Z	2389.9(4), 2	4281(6), 4	4537.4(10), 4
D_c/Mg m^{-3}	1.394	1.720	1.498
μ/mm^{-1}	0.695	1.526	0.977
F(000)	1034	2252	2114
Crystal size/mm	0.20 × 0.20 × 0.20	0.10 × 0.10 × 0.01	0.70 × 0.30 × 0.05
θ range for data collection/°	2.53–22.98	2.57–23.01	2.51–24.01
Limiting indices	$0 < h < 13$, $-21 < k < 21$, $-11 < l < 11$	$0 < h < 12$, $0 < k < 23$, $-18 < l < 18$	$0 < h < 14$, $0 < k < 25$, $-18 < l < 18$
Reflections collected	6679	6273	7473
Independent reflections	6289 [R(int) = 0.0399]	5943 [R(int) = 0.0366]	7118 [R(int) = 0.0323]
Observed reflections [$I > 2\sigma(I)$]	4338	3758	5097
Absorption correction	None	Semiempirical from ψ scans	None
Refinement method	Full-matrix least squares on F^2, (SHELXL 93)	Full-matrix least squares on F^2 (SHELXL 93)	Full-matrix least squares on F^2 (SHELXL 93)
Data, parameters	6266, 509	5943, 550	7071, 599
Goodness-of-fit on F^2	1.000	1.029	0.996
Final R indices [$I > 2\sigma(I)$] *	$R1 = 0.1009$, $wR2 = 0.2803$	$R1 = 0.0434$, $wR2 = 0.1121$	$R1 = 0.0538$, $wR2 = 0.1571$
R indices (all data) *	$R1 = 0.1447$, $wR2 = 0.3522$	$R1 = 0.1030$, $wR2 = 0.1339$	$R1 = 0.0931$, $wR2 = 0.2684$
Maximum/minimum electron density/e Å^{-3}	1.086, −1.047	0.784, −0.789	1.004, −0.892

* $wR2 = \{\Sigma[w(F_o^2 - F_c^2)^2]/\Sigma[w(F_o^2)^2]\}^{\frac{1}{2}}$.

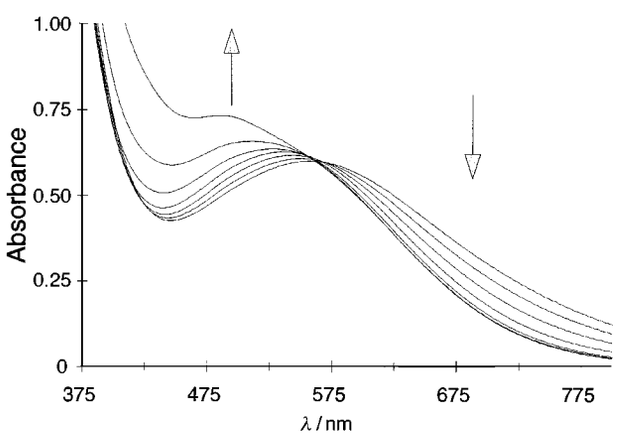

Fig. 1 The UV/VIS spectra in the range 375–800 nm of 1 : 5 v/v ethanol–water solutions of 1 mM Hbpbp and 2 mM iron(III) perchlorate. The arrows indicate the trend in spectral changes accompanying an increase in pH from 3 to 6.

not be isolated. This is not surprising if species of the type [(bpbp)$Fe_2(OH)_n(H_2O)_{4-n}$]$^{(4-n)+}$ are present. Indeed, since the complex [(bpbp)$Fe_2(F)_2(H_2O)_2$][BF_4]$_2$, see below, was successfully crystallized it seems reasonable to assume that the isoelectronic hydroxo complex cation [(bpbp)$Fe_2(OH)_2(H_2O)_2$]$^{2+}$ should be accessible, at least in solution. The color of the solution containing Hbpbp and iron perchlorate is also pH dependent; above approximately pH 5 the color is brown-red (the color of the putative tetranuclear complex isolated), between pH 2.5 and 5, purple, and below pH 2.5 blue. Fig. 1 shows the UV/VIS spectra of 1 : 2 mixtures of Hbpbp and iron perchlorate in water as a function of pH in a 1 : 5 v/v ethanol–water solution. Up to approximately pH 5.5 the spectra indicate the presence of two related species, as evidenced by the observation of two isosbestic points in the spectra between 375 and 800 nm. Above pH 5.5 a species independent of the others is formed. At low pH we assume the presence of the dimetallic species [(bpbp)$Fe_2(OH)_n(H_2O)_{4-n}$]$^{(4-n)+}$ (n = 0–2). A change in the integrity of the complex above pH 5 would be consistent with the formation of a tetranuclear species. Perhaps more than one or two terminal hydroxide ligands cannot be stabilized in these systems and dimerization/oligomerization ensues at pH values above 5. A strong band at 483 nm at pH > 5.5 is reminiscent of an oxide to Fe^{III} charge transfer band, and as such, consistent with the formulation of the red product as a tetranuclear ferric complex containing oxide bridging ligand(s).

Model complexes for the inhibitor complexes of PAPs

Fluoride complex. The reaction of Hbpbp with 2 equivalents of iron(II) tetrafluoroborate in methanol–water or acetone–water leads to the formation of purple-red solutions. On standing for several days, dark blue crystals of the mixed-valent complex [(bpbp)$Fe_2(F)_2(H_2O)_2$][BF_4]$_2$ are obtained. The complex of formula [(bpbp)$Fe_2(F)_2(H_2O)_2$][BF_4]$_2$ was difficult to distinguish from that of the isoelectronic (and desired) hydroxo complex [(bpbp)$Fe_2(OH)_2(H_2O)_2$][BF_4]$_2$, even after the crystal-structure determination. The co-ordinated fluoride ions in this complex are apparently derived from an abstraction of fluoride from the BF_4^- counter anions. This phenomenon has been noted previously for a series of copper–imidazole complexes by Reedijk and co-workers[21] who concluded that a fluoride ligand always needs to be stabilized by more than one metal ion or by one or more hydrogen bonds. Fluorine-19 NMR spectroscopy confirms the presence of both co-ordinated fluoride (δ 75.8) and fluoride in the counter anion (δ 3.2). The signal due to the Fe^{III} bound fluoride ions is very broad due to co-ordination to the paramagnetic centre. The Mössbauer spectrum of [(bpbp)-

Table 2 Selected bond distances (Å) and angles (°) for the cations in $[(bpbp)Fe_2(F)_2(H_2O)_2][BF_4]_2\cdot 4H_2O$ **1**, $[(bpbp)FeCu(CH_3CO_2)_2][ClO_4]_2\cdot 0.5CH_3OH$ **3** and the complex $[(bpbp)FeZn(MoO_4)_2]\cdot C_3H_7OH\cdot 2H_2O$ **2**

Complex **1**

Fe(1)–O(3)	2.027(9)	Fe(1)–N(2)	2.135(8)	Fe(2)–F(1)	2.000(7)	Fe(2)–N(3)	2.137(8)
Fe(1)–O(2)	2.059(8)	Fe(1)–N(5)	2.146(8)	Fe(2)–O(1)	2.033(6)	Fe(2)–N(4)	2.156(8)
Fe(1)–N(1)	2.116(9)	Fe(1)–O(1)	2.175(6)	Fe(2)–F(2)	2.106(7)	Fe(2)–N(6)	2.166(8)
O(3)–Fe(1)–O(2)	93.0(3)	N(2)–Fe(1)–N(5)	77.4(3)	F(1)–Fe(2)–F(2)	96.3(3)	N(3)–Fe(2)–N(4)	93.8(3)
O(3)–Fe(1)–N(1)	93.4(3)	O(3)–Fe(1)–O(1)	93.9(3)	O(1)–Fe(2)–F(2)	100.3(2)	F(1)–Fe(2)–N(6)	91.7(3)
O(3)–Fe(1)–N(2)	98.4(3)	O(2)–Fe(1)–O(1)	88.2(3)	O(1)–Fe(2)–N(3)	85.4(3)	O(1)–Fe(2)–N(6)	92.4(3)
O(2)–Fe(1)–N(2)	86.4(3)	N(1)–Fe(1)–O(1)	84.7(3)	F(2)–Fe(2)–N(3)	94.5(3)	N(3)–Fe(2)–N(6)	78.4(3)
N(1)–Fe(1)–N(2)	99.3(3)	N(5)–Fe(1)–O(1)	91.0(3)	F(1)–Fe(2)–N(4)	88.3(3)	N(4)–Fe(2)–N(6)	74.9(3)
O(2)–Fe(1)–N(5)	93.9(3)	F(1)–Fe(2)–O(1)	90.3(2)	F(2)–Fe(2)–N(4)	92.6(3)	Fe(2)–O(1)–Fe(1)	124.6(3)
N(1)–Fe(1)–N(5)	80.3(3)						

Complex **2**

Zn(1)–O(4)	1.964(5)	Zn(1)–N(6)	2.221(6)	Fe(1)–O(1)	2.156(5)	Mo(1)–O(2)	1.796(6)
Zn(1)–O(2)	2.042(5)	Fe(1)–O(5)	1.969(5)	Fe(1)–N(5)	2.221(6)	Mo(2)–O(9)	1.735(6)
Zn(1)–O(1)	2.104(5)	Fe(1)–O(3)	2.000(6)	Mo(1)–O(6)	1.720(6)	Mo(2)–O(8)	1.738(6)
Zn(1)–N(4)	2.145(6)	Fe(1)–N(1)	2.146(7)	Mo(1)–O(7)	1.734(6)	Mo(2)–O(3)	1.780(5)
Zn(1)–N(3)	2.163(6)	Fe(1)–N(2)	2.152(7)	Mo(1)–O(5)	1.793(5)	Mo(2)–O(4)	1.782(5)
O(4)–Zn(1)–O(2)	97.3(2)	O(2)–Zn(1)–N(6)	94.7(2)	O(3)–Fe(1)–N(2)	84.1(2)	N(1)–Fe(1)–N(5)	78.0(2)
O(4)–Zn(1)–O(1)	100.1(2)	O(1)–Zn(1)–N(6)	89.7(2)	N(1)–Fe(1)–N(2)	94.5(3)	N(2)–Fe(1)–N(5)	75.9(2)
O(2)–Zn(1)–O(1)	89.3(2)	N(4)–Zn(1)–N(6)	75.8(2)	O(5)–Fe(1)–O(1)	98.5(2)	O(1)–Fe(1)–N(5)	87.1(2)
O(4)–Zn(1)–N(4)	95.1(2)	N(3)–Zn(1)–N(6)	78.0(2)	O(3)–Fe(1)–O(1)	89.8(2)	Zn(1)–O(1)–Fe(1)	127.4(2)
O(2)–Zn(1)–N(4)	86.6(2)	O(5)–Fe(1)–O(3)	94.9(2)	N(1)–Fe(1)–O(1)	89.1(2)	Mo(1)–O(2)–Zn(1)	139.1(3)
O(4)–Zn(1)–N(3)	90.3(2)	O(5)–Fe(1)–N(1)	92.8(3)	N(2)–Fe(1)–O(1)	61.4(2)	Mo(1)–O(5)–Fe(1)	129.1(3)
O(2)–Zn(1)–N(3)	172.2(2)	O(3)–Fe(1)–N(1)	72.3(3)	O(5)–Fe(1)–N(5)	69.3(2)	Mo(2)–O(4)–Zn(1)	130.6(3)
O(1)–Zn(1)–N(3)	88.0(2)	O(5)–Fe(1)–N(2)	99.5(2)	O(3)–Fe(1)–N(5)	94.3(2)	Mo(2)–O(3)–Fe(1)	142.8(3)
N(4)–Zn(1)–N(3)	94.2(2)						

Complex **3**

Cu(1)–O(4)	1.960(4)	Cu(1)–N(6)	2.121(5)	Fe(1)–O(5)	1.934(4)	Fe(1)–N(5)	2.120(5)
Cu(1)–O(1)	2.006(3)	Cu(1)–O(2)	2.178(4)	Fe(1)–O(1)	1.984(3)	Fe(1)–O(3)	2.142(5)
Cu(1)–N(4)	2.066(4)	Cu(1)–N(3)	2.200(5)	Fe(1)–N(2)	2.071(4)	Fe(1)–N(1)	2.186(5)
O(4)–Cu(1)–O(1)	98.9(2)	O(4)–Cu(1)–N(3)	92.0(2)	N(2)–Fe(1)–N(5)	78.2(2)	N(2)–Fe(1)–N(1)	96.7(2)
O(4)–Cu(1)–N(4)	93.6(2)	O(1)–Cu(1)–N(3)	86.6(2)	O(5)–Fe(1)–O(3)	92.3(2)	N(5)–Fe(1)–N(1)	80.0(2)
O(1)–Cu(1)–N(6)	89.7(2)	N(4)–Cu(1)–N(3)	96.6(2)	O(1)–Fe(1)–O(3)	89.2(2)	Fe(1)–O(1)–Cu(1)	118.0(2)
N(4)–Cu(1)–N(6)	78.6(2)	N(6)–Cu(1)–N(3)	80.3(2)	N(2)–Fe(1)–O(3)	85.6(2)	C(9)–O(2)–Cu(1)	131.4(4)
O(4)–Cu(1)–O(2)	92.8(2)	O(5)–Fe(1)–O(1)	99.0(2)	N(5)–Fe(1)–O(3)	95.0(2)	C(9)–O(5)–Fe(1)	134.4(4)
O(1)–Cu(1)–O(2)	88.4(2)	O(5)–Fe(1)–N(2)	93.0(2)	O(5)–Fe(1)–N(1)	93.2(2)	C(7)–O(4)–Cu(1)	132.9(4)
N(4)–Cu(1)–O(2)	87.4(2)	O(1)–Fe(1)–N(5)	90.6(2)	O(1)–Fe(1)–N(1)	87.4(2)	C(7)–O(3)–Fe(1)	133.4(5)
N(6)–Cu(1)–O(2)	95.6(2)						

$Fe_2(F)_2(H_2O)_2][BF_4]_2$ **1** recorded at 80 K confirms mixed valency. The quadrupole doublet parameters for the high-spin Fe^{2+} are ΔE_Q, 3.242 mm s^{-1} and δ, 1.169 mm s^{-1}, and for the high spin Fe^{3+} are ΔE_Q, 0.221 mm s^{-1} and δ, 0.460 mm s^{-1}.

The inhibition by fluoride ions at the active site of PAPs occurs after substitution of a co-ordinated water molecule.[22] No structural data using single-crystal methods or EXAFS to analyze fluoride inhibited PAP have been reported. Thus neither the mode of active site binding nor the number of bound fluoride ions is established. Crowder and co-workers[15b,22] have carried out kinetic and EPR studies of the reaction of BSPAP with excess fluoride, so the number of fluoride ions that can be bound at the active site of BSPAP was not ascertained in this study. Our complex suggests that fluoride ions will, perhaps not unexpectedly, be bound to the iron(III) atom in PAPs and that such terminally bound fluoride ion could be stabilized by intramolecular hydrogen bonding to water ligands bound to the adjacent divalent metal ion. In the absence of such intramolecular binding, fluoride ions may bridge between the metal centers.

Molybdate complex. The neutral bis(molybdate)-bridged heterodimetallic iron(III)–zinc(II) complex, $(bpbp)FeZn(MoO_4)_2$, was prepared in quantitative yields. To our knowledge this is the first report of molybdate bridging between two different metal ions, and suggests that this bridging mode may be operative in molybdate inhibited PAP. A bidentate bridging mode for the tetrahedral oxo anions was evident in the recent crystal structures of WO_4^{2-}- and PO_4^{2-}-bound RKBPAP.[3b] While the structure of $(bpbp)FeZn(MoO_4)_2$ demonstrates the ability of the molybdate ion to form a bidentate bridge between an iron and a zinc atom, the presence of two molybdate bridges does not directly accord with the reported single-molybdate binding mode in PAPs. The uptake of one or two molybdate bridging groups by both PAPs and model complexes such as the present one might, however, be feasible depending on the electric charge distribution in the complexes, the presence of other negatively-charged ligands and the steric requirements of the surrounding cavity.

Hydrolysis of alkyl esters to give acetate-bridged complexes

A series of bis(acetate)-bridged complexes were obtained by a novel method as illustrated in Scheme 1. The complexes $[(bpbp)FeM(CH_3CO_2)_2][ClO_4]_2$ (M = Co, Ni, Cu, Zn or Fe) precipitated as crystalline solids after the diffusion of ethyl acetate into aqueous mixtures containing Hbpbp, 1 equivalent of either Fe^{3+} or Fe^{2+} (as perchlorate salts) and 1 equivalent of a divalent metal ion (as the perchlorate salt). The acetate bridges must be derived from the hydrolysis of ethyl acetate. The complexes are apparently formed slowly and require standing over a period of at least 24 h at room temperature. The crystal structure of a representative complex is described below.

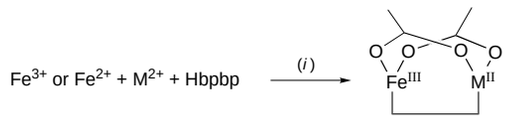

Scheme 1 M = Fe, Co, Cu, Ni or Zn. (*i*) H_2O–MeOH, $MeCO_2Et$ or $MeCO_2Pr^i$

In all cases the ES mass spectra showed that the heterodimetallic complexes are homogeneous: no peaks assignable to the corresponding homodimetallic complexes are observed. At present we are unable to establish whether or not the hydrolysis of ethyl acetate is promoted by the metal complexes or whether the background hydrolysis of the ester occurs at sufficient levels to provide enough acetate ions for the quantitative formation of these compounds. Convincing proof that this is a dimetal-promoted reaction would be of tremendous importance with respect to modelling the functional chemistry of PAPs. The same series of complexes was also obtained using the more hydrolytically stable isopropyl acetate.

As noted above the dimetal-catalysed hydrolyses of nitriles, carboxamides and phosphate esters have been reported, however, there are no such reports of corresponding reactions with alkyl esters. In the light of these results we have tested other substrates for their possible hydrolytic reactivity in the presence of $[(bpbp)FeM]^{4+}$, however, we have found no evidence to suggest that the hydrolysis of nitriles, aryl acetates or phosphate mono- or di-esters is enhanced above the level of spontaneous hydrolysis in the presence of the mixtures described above.‡

X-Ray crystal structures

The structures of the cations in $[(bpbp)Fe_2(F)_2(H_2O)_2][BF_4]_2\cdot 4H_2O$ **1** and $[(bpbp)FeCu(CH_3CO_2)_2][ClO_4]_2\cdot 0.5CH_3OH$ **3** and the complex in $[(bpbp)FeZn(MoO_4)_2]\cdot C_3H_7OH\cdot 2H_2O$ **2** are depicted in Figs. 2, 4 and 3. The structures of the cations in all three complexes are similar and all asymmetrical. The cation $[(bpbp)Fe_2(F)_2(H_2O)_2]^{2+}$ shows the greatest asymmetry, not only due to different co-ordination spheres for the two metal ions but also because of the very asymmetric bonding arrangement around the hinging phenolate oxygen atom with a difference of 0.14 Å between the two Fe–O(1) distances. Assignments of the trivalent and divalent ions are based on the bond distances around the metal ions. Assignment of the oxygen atoms of the waters bound to iron(II) [Fe(1)] and the fluoride ions bound to iron(II) [Fe(2)] was made using similar criteria, although it was not possible to locate the hydrogen atoms. The two fluoride ions attached to Fe(2) are, however, within hydrogen-bonding distance from the two water ligands on Fe(1) with F(1)···O(3) 2.676(11), F(2)···O(2) 2.817(10) Å. The O(2)···O(3) distance of 2.964(10) Å is also within hydrogen-bonding range. This hydrogen-bonding network extends to the four crystal water molecules located between pairs of diiron units over five positions with five O···O distances of between 2.6 and 2.9 Å found in the electron density map.

‡ The hydrolysis of *p*-nitrophenyl acetate, *p*-nitrophenyl phosphate and bis(*p*-nitrophenyl) phosphate at pH ranging from 1.5 to 9 and at 25 °C was followed by monitoring the release of *p*-nitrophenolate spectrophotometrically. The reaction solution was made by adding 0.500 cm^3 of a stock solution of 3.0 mM Hbpbp and 6.0 mM iron(III) perchlorate [or iron(II) tetrafluoroborate] in acetone to 10.000 cm^3 of a 0.100 M $NaClO_4$ solution in water which was 1.4 mM in the substrate. In order to avoid any interference from a buffer an automated titrator (TTT11b) connected to a modified autoburette and a combined pH electrode, all from Radiometer, Denmark, was used with either 1.0 mM NaOH or 1.0 mM $HClO_4$ to ensure a constant pH. At appropriate time intervals 0.100 cm^3 aliquots of the reaction solution were quenched with 0.900 cm^3 of 0.100 M NaO_2CMe in a 10 mM 4-(2-hydroxyethyl)-1-piperazineethanesulfonic acid (HEPES) buffer at pH 8.5. The generated *p*-nitrophenolate was measured at 405 nm.

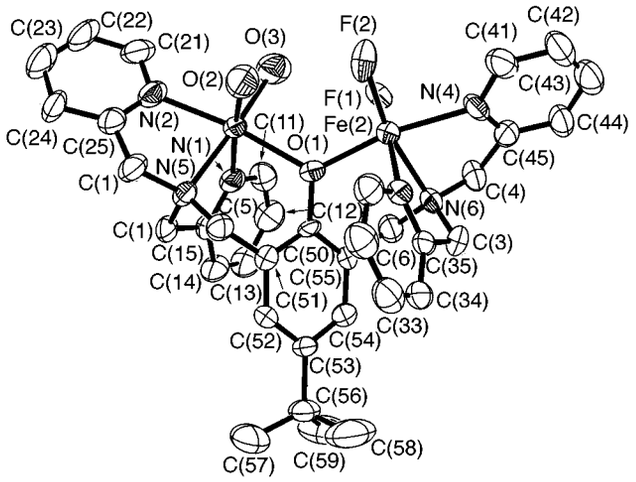

Fig. 2 The molecular arrangement of the cation in $[(bpbp)Fe_2(F)_2(H_2O)_2][BF_4]_2\cdot 4H_2O$ **1**

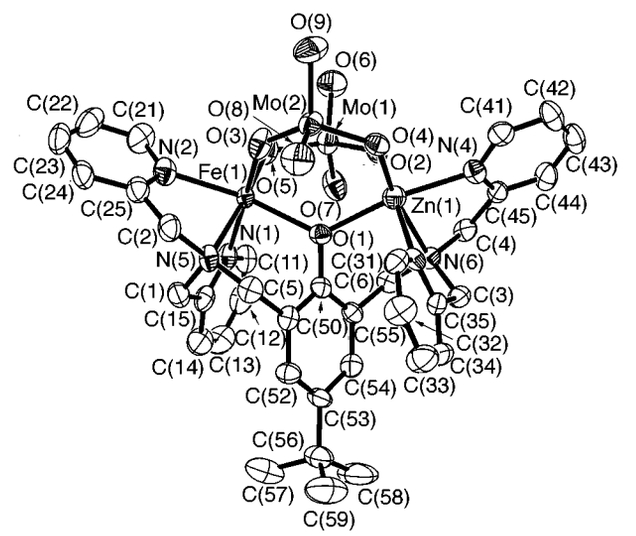

Fig. 3 The molecular arrangement of $[(bpbp)FeZn(MoO_4)_2]\cdot C_3H_7OH\cdot 2H_2O$ **2**, solvent molecules omitted for clarity

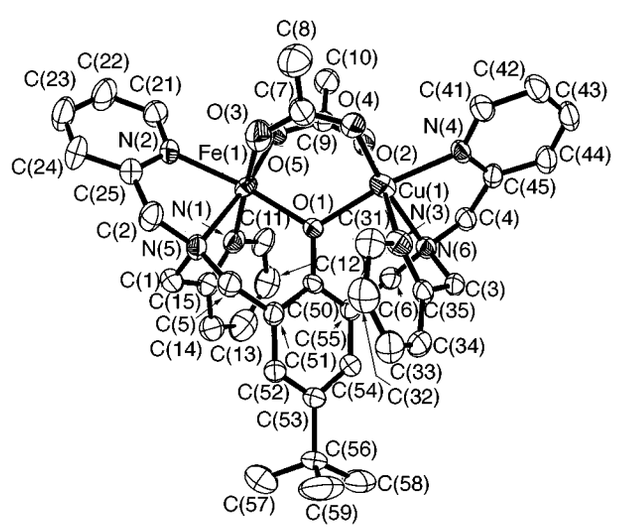

Fig. 4 The molecular arrangement of the cation in $[(bpbp)FeCu(CH_3CO_2)_2][ClO_4]_2\cdot 0.5CH_3OH$ **3**

The Fe···Fe, Fe···Zn and Fe···Cu separations are 3.726(2), 3.819(4) and 3.419(2) Å in $[(bpbp)Fe_2(F)_2(H_2O)_2]^{2+}$, $[(bpbp)FeZn(MoO_4)_2]$ and $[(bpbp)FeCu(CH_3CO_2)_2]^{2+}$ respectively. Recently a phenolate-hinged diiron complex with Fe···Fe of 3.193(2) Å was reported with an exogenous methoxide as

Table 3 Redox potentials for $[(bpbp)FeM(CH_3CO_2)_2]^{2+}$ (M = Fe, Zn, Cu, Ni or Co)

Compound	$E_{\frac{1}{2}}$/mV
$[(bpbp)Fe_2(CH_3CO_2)_2][ClO_4]_2$	386 ($Fe^{III}Fe^{III}/Fe^{III}Fe^{II}$)
	−334 ($Fe^{III}Fe^{II}/Fe^{II}Fe^{II}$)
$[(bpbp)FeZn(CH_3CO_2)_2][ClO_4]_2$	−334 ($Fe^{III}Zn^{II}/Fe^{II}Zn^{II}$)
$[(bpbp)FeCu(CH_3CO_2)_2][ClO_4]_2$	−308 ($Fe^{III}Cu^{II}/Fe^{II}Cu^{II}$)
$[(bpbp)FeNi(CH_3CO_2)_2][ClO_4]_2$	−389 ($Fe^{III}Ni^{II}/Fe^{II}Ni^{II}$)
$[(bpbp)FeCo(CH_3CO_2)_2][ClO_4]_2$	−352 ($Fe^{III}Co^{II}/Fe^{II}Co^{II}$)

bridging group.[23] To the best of our knowledge the largest metal–metal separation for such a system was reported for a phenolate-hinged Cu^{II}–V^{IV} complex [3.907(2) Å].[2k] Thus metal–metal separations ranging from at least 3.193(2) to 3.907(2) Å are attainable in acyclic phenolate-hinged dimetallic complexes making these systems very flexible in the type of bridging and 'non-bridging' groups that can be incorporated at the exogenous site. This fact may be of some importance for the use of this class of complex as homogeneous catalysts for processes involving the condensation of species which have been selectively bound at each metal ion.

Electrochemistry

Results from the cyclic voltammetry experiments with the series of complexes $[(bpbp)FeM(CH_3CO_2)_2][ClO_4]_2$ (M = Co, Ni, Cu, Zn or Fe) are listed in Table 3. All the heterometallic complexes exhibited a single reversible one-electron wave due to the iron(III) ion. The mixed-valence diiron complex exhibited two reversible one-electron waves. Chemical reversibility was substantiated in all experiments by (*i*) a ΔE_p value of 60–70 mV, (*ii*) the $E_{\frac{1}{2}}$ values were independent of the scan rate from 25 to 150 mV s^{-1}, (*iii*) $i_c/i_a \approx 1$ and (*iv*) the peak current was proportional to the square root of the scan rate.

The low-potential $E_{\frac{1}{2}}$ of the Fe center depends only insignificantly on the nature of the second metal ion. This is interesting and suggests that the interaction between the two centers is dominated by the overall charges rather than by details of the electronic structure. The wave separation of the diiron complex, $\Delta E_{\frac{1}{2}}$, is large (720 mV). This is indicative that the electrostatic feature is strong and only weakly screened by the external solvent. An 'effective' relative permittivity would thus be 3–4, in comparison with the bulk value of 37 for acetonitrile.

The equilibrium constant, K_{com}, for the comproportionation equilibrium (1) was calculated from the cyclic voltammetric

$$[(bpbp)Fe^{II}Fe^{II}(CH_3CO_2)_2]^+ + [(bpbp)Fe^{III}Fe^{III}(CH_3CO_2)_2]^{3+} \Longleftrightarrow 2\,[(bpbp)Fe^{III}Fe^{II}(CH_3CO_2)_2]^{2+} \quad (1)$$

analysis, since $K_{com} = \exp[(nF)E/RT]$, where $E = E_{\frac{1}{2}}(Fe^{III}Fe^{III}/Fe^{III}Fe^{II}) - E_{\frac{1}{2}}(Fe^{III}Fe^{II}/Fe^{II}Fe^{II})$. For $[(bpbp)Fe_2(CH_3CO_2)_2][ClO_4]_2$ the value for ΔE_p is 720 mV, which yields a K_{com} value of 1.5×10^{12}.

Satisfactory cyclic voltammograms could not be obtained for either $[(bpbp)Fe_2(F)_2(H_2O)_2][BF_4]_2$ or $[(bpbp)FeZn(MoO_4)_2]$ under the conditions described in the Experimental section.

Spectroelectrochemistry

Spectroelectrochemical measurements were recorded for $[(bpbp)Fe_2(CH_3CO_2)_2][ClO_4]_2$ and $[(bpbp)FeZn(CH_3CO_2)_2][ClO_4]_2$ in dry acetonitrile. Fig. 5 shows the sequences of background corrected spectroelectrochemical recordings for the $Fe^{III}Fe^{II} \Longleftrightarrow Fe^{II}Fe^{II}$ and the $Fe^{III}Zn^{II} \Longleftrightarrow Fe^{II}Zn^{II}$ transitions in the potential range from −750 mV to 0 mV (*vs.* the Ag–$AgNO_3$ reference electrode). The following spectral features on conversion from the oxidized to the reduced form are notable.

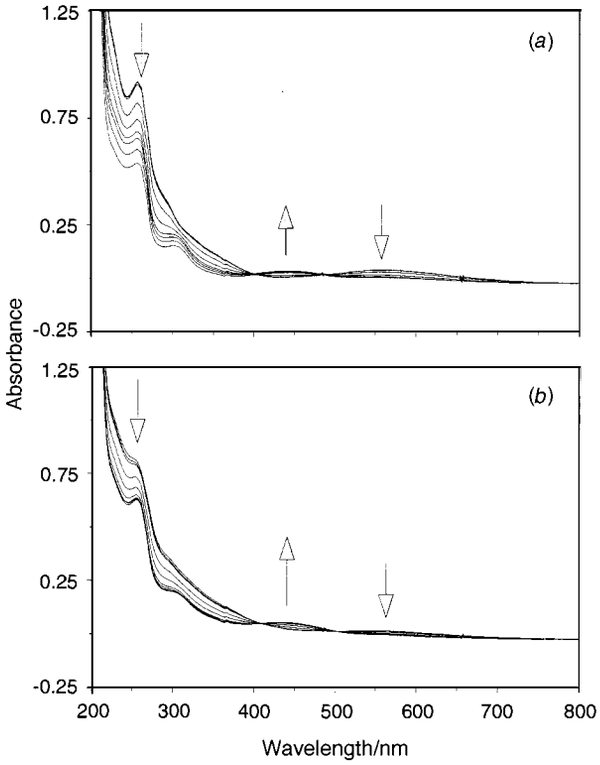

Fig. 5 Spectral changes accompanying the $Fe^{III} \Longleftrightarrow Fe^{II}$ transition in (*a*) $[(bpbp)FeZn(CH_3CO_2)_2][ClO_4]_2$ and (*b*) $[(bpbp)Fe_2(CH_3CO_2)_2][ClO_4]_2$. Arrows indicate the spectral trends upon reduction

(*i*) The two complexes follow very similar patterns. (*ii*) The most conspicuous feature is that the visible 432 nm band builds up whereas the 555 nm band disappears on reduction of the $Fe^{III}Fe^{II}$ complex. These bands are located at 445 nm and 558 nm, respectively, and behave similarly for the $Fe^{III}Zn^{II}$ system. The two bands are most likely metal-to-ligand and ligand-to-metal charge-transfer transitions, respectively but further analysis of this issue is not available presently. (*iii*) The two sets of isosbestic points support the single-electron nature of the transitions. (*iv*) Various transitions in the UV spectral region can be distinguished. These are enhanced approximately twice upon oxidation and can therefore also be associated with ligand-to-metal charge transfer.

Very little spectral change on the $Fe^{III}Fe^{II}$ complex could be determined in the potential range from 0 to 750 mV. This range envelopes the oxidation potential for the $Fe^{III}Fe^{II} \longrightarrow Fe^{III}Fe^{III}$ oxidation observed in the cyclic voltammograms, and further systematic changes in both the visible and UV spectral regions might have been anticipated. Surface oxidation and passivation of the transparent gold film working electrode is a possible reason for this observation.

Acknowledgements

We are grateful to Henrik Molina Svendsen for recording electrospray mass spectra. This work was supported by a Ph.D. grant (to M. G.) and grant no. 9503162 (to C. J. M.) from the Danish Natural Science research council and the Wellcome Trust (to A. K. P.).

References

1 H.-R. Chang, S. K. Larsen, P. D. W. Boyd, C. G. Pierpont and D. N. Hendrickson, *J. Am. Chem. Soc.*, 1988, **110**, 4565; C. Fraser, L. Johnston, A. L. Rheingold, B. S. Haggerty, G. K. Williams, J Whelan and B. Bosnich, *Inorg. Chem.*, 1992, **31**, 1835.

2 (*a*) M. Suzuki, M. Mikuriya, S. Murata, A. Uehara and H. Oshio, *Bull. Chem. Soc. Jpn.*, 1987, **60**, 4305; (*b*) A. S. Borovik and L. Que, jun., *J. Am. Chem. Soc.*, 1988, **110**, 2345; (*c*) H. Diril, H.-R. Chang,

M. J. Nilges, X. Zhang, J. A. Potenza, H. J. Schugar, D. N. Hendrickson and S. S. Isied, *J. Am. Chem. Soc.*, 1988, **110**, 625; (*d*) R. M. Buchanan, K. J. Oberhausen and J. F. Richardson, *Inorg. Chem.*, 1988, **27**, 971; (*e*) H. Diril, H.-R. Chang, M. J. Nilges, X. Zhang, J. A. Potenza, H. J. Schugar, S. S. Isied and D. N. Hendrickson, *J. Am. Chem. Soc.*, 1988, **111**, 5102; (*f*) A. S. Borovik, V. Papaefthymiou, L. F. Taylor, O. P. Anderson and L. Que, jun., *J. Am. Chem. Soc.*, 1989, **111**, 6183; (*g*) T. R. Holman, C. Juarez-Garcia, M. P. Hendrich, L. Que, jun. and E. Münck, *J. Am. Chem. Soc.*, 1990, **112**, 7611; (*h*) M. S. Mashuta, R. J. Webb, J. K. McCusker, E. A. Schmitt, K. J. Oberhausen, J. F. Richardson, R. M. Buchanan and D. N. Hendrickson, *J. Am. Chem. Soc.*, 1992, **114**, 3815; (*i*) W. Kanda, W. Moneta, M. Bardet, E. Bernard, N. Debaecker, J. Laugier, A. Boussekou, S. Chardon-Noblat and J.-M. Latour, *Angew. Chem., Int. Ed. Engl.*, 1995, **34**, 588; (*j*) A. Neves, M. A. de Brito, I. Vencato, V. Drago, K. Griesar and W. Haase, *Inorg. Chem.*, 1996, **35**, 2360; (*k*) A. Hazell, C. J. McKenzie, B. Moubaraki and K. Murray, *Acta Chem. Scand.*, 1997, **51**, 470.

3 (*a*) N. Sträter, T. Klabunde, P. T. Tucker, H. Witzel and B. Krebs, *Science*, 1995, **268**, 1489; (*b*) T. Klabunde, N. Sträter, R. Frölich, H. Witzel and B. Krebs, *J. Mol. Biol.*, 1996, **259**, 737.

4 A. Hazell, K. B. Jensen, C. J. McKenzie and H. Toftlund, *Inorg. Chem.*, 1994, **33**, 3127.

5 D. R. Jones, L. F. Lindoy and A. M. Sargeson, *J. Am. Chem. Soc.*, 1984, **106**, 7807; P. Hendry and A. M. Sargeson, *Prog. Inorg. Chem.*, 1990, **38**, 201; J. Chin, *Acc. Chem. Res.*, 1991, **24**, 145.

6 Y. Dong, H. Fujii, M. P. Hendrich, R. A. Leising, G. Pan, C. R. Randall, E. C. Wilkinson, Y. Zang, L. Que, jun., B. G. Fox, K. Kauffman and E. Münck, *J. Am. Chem. Soc.*, 1995, **117**, 2778; K. D. Hodges, R. G. Wollman, S. L. Kessel, D. N. Hendrickson, D. G. VanDerveer and E. K. Barefield, *J. Am. Chem. Soc.*, 1979, **101**, 906; J. W. Buchler, K. L. Lay, Y. J. Lee and W. R. Scheidt, *Angew. Chem., Int. Ed. Engl.*, 1982, **21**, 432.

7 M. J. Young and J. Chin, *J. Am. Chem. Soc.*, 1995, **117**, 10 577; N. N. Murthy, M. Mahroof-Tahir and K. D. Karlin, *J. Am. Chem. Soc.*, 1993, **115**, 10 404.

8 W. H. Chapman, jun. and R. Breslow, *J. Am. Chem. Soc.*, 1995, **117**, 5462; M. Yashiro, A. Ishikubo and M. Komiyama, *J. Chem. Soc., Chem. Commun.*, 1995, 1793.

9 C. J. McKenzie and R. Robson, *J. Chem. Soc., Chem. Commun.*, 1988, 112.

10 A. Tsubouchi and T. C. Bruice, *J. Am. Chem. Soc.*, 1994, **116**, 11 614.

11 N. Sträter, W. N. Lipscomb, T. Klabunde and B. Krebs, *Angew. Chem., Int. Ed. Engl.*, 1996, **35**, 2024; B. A. Averill, *Biochemistry*, 1992, **31**, 3033; J. B. Vincent, M. W. Crowder and B. A. Averill, *TIBS*, 1992, **17**, 105.

12 J. E. Coleman, *Annu. Rev. Biophys. Biomol. Struct.*, 1992, **21**, 441.

13 N. E. Dixon, P. W. Riddles, C. Gazzola, R. L. Blakeley and B. Zerner, *Can. J. Biochem.*, 1980, **58**, 1335.

14 J. S. Seo, N.-D. Sung, R. C. Hynes and J. Chin, *Inorg. Chem.*, 1996, **35**, 7472.

15 (*a*) J. C. Davis, S. S. Lin and B. A. Averill, *Biochemistry*, 1981, **20**, 4062; (*b*) J. B. Vincent, M. W. Crowder and B. A. Averill, *Biochemistry*, 1991, **30**, 3025.

16 B. F. Hoskins, C. J. McKenzie, R. Robson and L. Zhenrong, *J. Chem. Soc., Dalton Trans.*, 1990, 2637.

17 W. R. Heineman, B. J. Norris and J. F. Goelz, *Anal. Chem.*, 1975, **47**, 79.

18 H. B. Gray, personal communication.

19 G. M. Sheldrick, SHELXTL PLUS, Siemens Analytical X-ray Instruments Inc., Madison, WI, 1990.

20 G. M. Sheldrick, SHELXL 93, Program for Crystal Structure Refinement, University of Göttingen, 1993.

21 J. Reedijk, *Comments Inorg. Chem.*, 1982, **1**, 379; J. Reedijk, R. W. M. ten Hoedt, *Recl. Trav. Chim. Pays-Bas*, 1982, **101**, 49; F. S. Keij, R. A. G. de Graaff, J. G. Haasnoot, A. J. Oosterling, E. Pedersen and J. Reedijk, *J. Chem. Soc., Chem. Commun.*, 1988, 423.

22 M. W. Crowder, J. B. Vincent and B. A. Averill, *Biochemistry*, 1992, **31**, 9603.

23 C. Belle, I. Gautier-Luneau, J.-L. Pierre, C. Scheer and E. Saint-Aman, *Inorg. Chem.*, 1996, **35**, 3706.

Received 23*rd June* 1997; *Paper* 7/04388K